Forging New Antibiotic Combinations under Iron-Limiting Conditions

Derek C. K. Chan,[a] Irene Guo,[a] Lori L. Burrows[a]

aDepartment of Biochemistry and Biomedical Sciences, Michael G. DeGroote Institute for Infectious Diseases Research, McMaster University, Hamilton, Ontario, Canada

ABSTRACT *Pseudomonas aeruginosa* is a multidrug-resistant nosocomial pathogen. We showed previously that thiostrepton (TS), a Gram-positive thiopeptide antibiotic, is imported via pyoverdine receptors and synergizes with iron chelator deferasirox (DSX) to inhibit the growth of *P. aeruginosa* and *Acinetobacter baumannii* clinical isolates. A small number of *P. aeruginosa* and *A. baumannii* isolates were resistant to the combination, prompting us to search for other compounds that could synergize with TS against those strains. From literature surveys, we selected 14 compounds reported to have iron-chelating activity, plus one iron analogue, and tested them for synergy with TS. Doxycycline (DOXY), ciclopirox olamine (CO), tropolone (TRO), clioquinol (CLI), and gallium nitrate (GN) synergized with TS. Individual compounds were bacteriostatic, but the combinations were bactericidal. Our spectrophotometric data and chrome azurol S agar assay confirmed that the chelators potentiate TS activity through iron sequestration rather than through their innate antimicrobial activities. A triple combination of TS plus DSX plus DOXY had the most potent activity against *P. aeruginosa* and *A. baumannii* isolates. One *P. aeruginosa* clinical isolate was resistant to the triple combination but susceptible to a triple combination containing higher concentrations of CLI, CO, or DOXY. All *A. baumannii* isolates were susceptible to the triple combinations. Our data reveal a diverse set of compounds with dual activity as antibacterial agents and TS adjuvants, allowing combinations to be tailored for resistant clinical isolates.

KEYWORDS thiostrepton, iron, *Pseudomonas aeruginosa*, *Acinetobacter baumannii*, chelator

Iron is a critical micronutrient for bacteria, influencing biofilm formation, pathogenicity, and growth (1, 2). The opportunistic Gram-negative pathogen *Pseudomonas aeruginosa* has an extensive repertoire of iron acquisition systems that are upregulated under iron-deplete conditions, similar to those encountered during infection. To overcome iron limitation, *P. aeruginosa* produces the iron-scavenging siderophores pyochelin and pyoverdine that bind iron with low and high affinity, respectively (3–5). Pyoverdine and its outer membrane receptors, FpvA and FpvB, are highly expressed under low-iron conditions (3, 6, 7). Pyoverdine has such a high binding affinity (10^{32} M^{-1}) for iron that it can strip it from transferrin, a mammalian protein responsible for sequestering iron to impede bacterial growth (8–11). Transcriptome sequencing (RNA-seq) data showed that pyoverdine biosynthetic enzymes and uptake are highly upregulated *in vivo* in response to the iron-deprived environment (7). *P. aeruginosa* deficient in iron uptake mechanisms are less able to cause infections than their wild-type counterparts (12).

Natural products often exploit iron acquisition pathways to cross the Gram-negative outer membrane. Pyocin S2, produced by *P. aeruginosa* to kill competing strains, and related toxins are taken up via FpvA (13, 14). The sideromycins, which resemble siderophores but have intrinsic antibacterial activity, also exploit iron uptake pathways

(15). Taking advantage of this phenomenon, several groups have created synthetic siderophore-beta-lactam conjugates to target Gram-negative bacteria, using the iron-binding group as a Trojan horse to deliver antibiotics (16–18). One such example is cefiderocol, a siderophore beta-lactam that recently completed phase III clinical trials. The catechol group of cefiderocol binds iron and the complex is taken up via PiuA, an outer membrane receptor for iron transport (18, 19, 68). The compound demonstrated potent activity against *Escherichia coli* and *Klebsiella pneumoniae* (19, 20). Thus, the Trojan horse approach enhances the delivery of antibiotics compared to diffusion alone.

Our group recently discovered that the thiopeptide antibiotic thiostrepton (TS) hijacks pyoverdine receptors under iron-limited conditions to cross the outer membranes of the World Health Organization's top two critical priority pathogens, *P. aeruginosa* and *Acinetobacter baumannii* (21). TS activity was potentiated in heat-inactivated mouse and human serum and by FDA-approved iron chelators, deferiprone (DFP) and deferasirox (DSX). However, a small number of *P. aeruginosa* and *A. baumannii* strains were resistant to TS-chelator combinations, prompting us to look for new compounds that could synergize with TS to inhibit those clinical isolates.

With the aim of finding compounds that could synergize with TS under iron-limiting conditions, we performed a literature search to identify bioactive iron chelators. We selected 14 putative iron-binding compounds as well as gallium, an iron analogue. Five compounds synergized with TS and had activity against *P. aeruginosa* and *A. baumannii* clinical isolates. Each compound was bacteriostatic against *P. aeruginosa* PA14; however, the addition of TS made the combination bactericidal. Growth of one highly resistant *P. aeruginosa* clinical isolate was inhibited with higher concentrations of three of the compounds in combination with TS plus DSX. These data identify a set of molecules of diverse structure and biological activity that synergize with TS, providing the ability to tailor combinations for resistant strains.

RESULTS

Iron-binding antibiotics form colored complexes. We first screened a panel of common antibiotics for potential iron-chelating activity using a qualitative assay, monitoring the change in color upon addition of $FeCl_3$. Binding of transition metals results in the formation of colored complexes that absorb the visible wavelengths of light, detectable by spectroscopy and by eye (22–24). The panel consisted of 22 antibiotics from the aminoglycoside, fluoroquinolone, beta-lactam, and tetracycline classes (Fig. 1). Iron chelators DFP and DSX served as positive controls, turning dark red/violet upon addition of ferric iron at a final concentration of 10 μM. The tetracyclines doxycycline (DOXY), tetracycline, and minocycline exhibited similar color changes. The fluoroquinolones ciprofloxacin, ofloxacin, and pipemidic acid formed orange complexes; however, the intensity of the color change was weaker than with the tetracyclines, DFP, and DSX. A number of beta-lactams showed color changes ranging from a brown-orange to red-orange. Ceftriaxone was the only beta-lactam that turned red in the presence of ferric iron. Trimethoprim turned golden yellow.

Binding of ferric iron shifts absorption spectra. To verify spectral shifts for compounds that changed color upon addition of ferric iron, a 96-well spectrophotometric assay was performed with final concentrations of antibiotic and $FeCl_3$ of 300 μM each. The absorption spectra were scanned from 300 to 700 nm. The spectra of ciprofloxacin (CIP), pipemidic acid, ofloxacin, tetracycline, minocycline, DOXY, DSX, and DFP shifted after the addition of $FeCl_3$ (Fig. 2), confirming the results of the qualitative assay. Chloramphenicol and ampicillin served as negative controls. The spectrum for ceftriaxone did not change at the concentrations tested, suggesting that the changes in color observed for beta-lactams were likely due to concentration effects.

Identification of other compounds that chelate iron. To expand our panel of potential chelators beyond known antibiotics, we searched the literature for bioactive compounds that were reported to have iron-chelating activity. We identified 14 compounds (Table 1) plus gallium nitrate (GN). Gallium is an iron analogue that inhibits
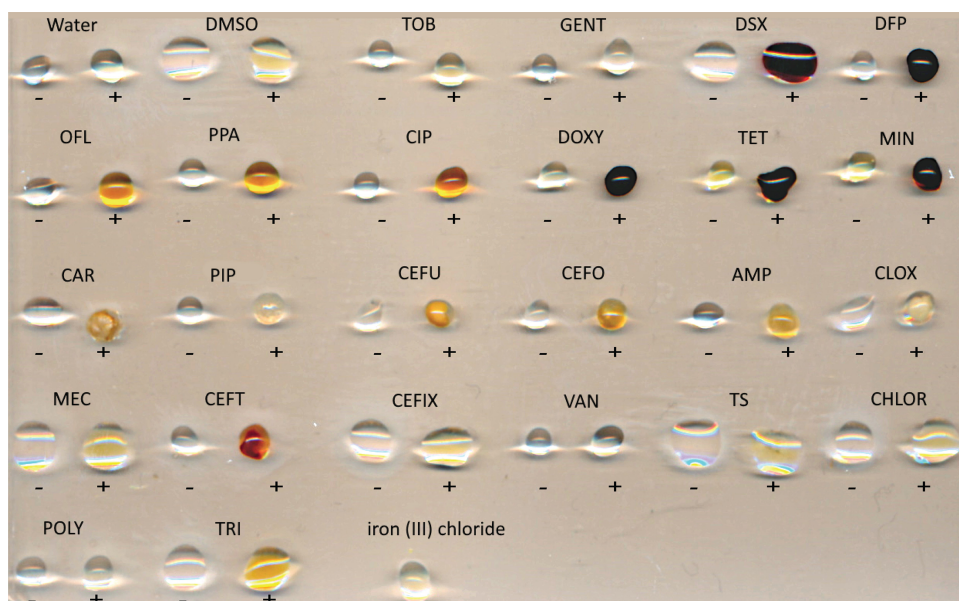
FIG 1 Qualitative assay to identify potential antibiotic-Fe^{3+} complexes. Binding of iron by a compound causes spectral shifts that can be detected visually. Five microliters of stock concentration antibiotic (listed below) was added to 5 μl of $FeCl_3$ to a final $FeCl_3$ concentration of 10 μM and incubated at room temperature for 1 h. Negative controls without iron are indicated by a minus sign and droplets with $FeCl_3$ are indicated with a plus sign. Vehicle controls with Milli-Q H_2O and DMSO were included. The concentrations of each antibiotic stock were as follows: TOB (tobramycin; 4 mg/ml), GENT (gentamicin; 10 mg/ml), DSX (deferasirox; 20 mg/ml), DFP (deferiprone; 60 mg/ml), OFL (ofloxacin; 4 mg/ml), PPA (pipemidic acid; 64 mg/ml), CIP (ciprofloxacin; 5 mg/ml), DOXY (doxycycline; 50 mg/ml), TET (tetracycline; 20 mg/ml), MIN (minocycline; 20 mg/ml), CAR (carbenicillin; 100 mg/ml), PIP (piperacillin; 6 mg/ml), CEFU (cefuroxime; 30 mg/ml), CEFO (cefotaxime; 30 mg/ml), AMP (ampicillin; 30 mg/ml), CLOX (cloxacillin; 30 mg/ml), MEC (amdinocillin; 30 mg/ml), CEFT (ceftriaxone; 30 mg/ml), CEFIX (cefixime; 12 mg/ml), VAN (vancomycin; 30 mg/ml), TS (thiostrepton; 20 mg/ml), CHLOR (chloramphenicol; 50 mg/ml), POLY (polymyxin B; 4 mg/ml), and TRI (trimethoprim; 50 mg/ml).

siderophore production, iron uptake, and the activity of enzymes that use iron (25). The spectrophotometric assay was repeated for all compounds listed in Table 1 except for clioquinol (CLI). CLI was identified in our previous screen as a *P. aeruginosa* growth inhibitor (21) but precipitated at concentrations >8 μg/ml. Ciclopirox olamine (CO) and tropolone (TRO) showed shifts in their absorption spectra (Fig. 2). A chrome azurol S (CAS) assay was also used to detect iron binding through decolorization of the blue agar, indicating removal of Fe^{3+} from the CAS–hexadecyl-trimethyl-ammonium bromide (HDTMA) complex (see Fig. S1 in the supplemental material). DSX, TRO, and CO showed the greatest decolorization and thus the highest relative affinity for iron. Interestingly, DOXY showed a marked color shift in the presence of Fe^{3+} (Fig. 2) but minimally decolorized CAS agar.

Numerous iron chelators synergize with TS. Based on their ability to bind iron, each compound from Table 1, as well as DOXY and CIP, were assessed for synergy with TS using checkerboard assays. DOXY, CO, CLI, TRO, and GN all synergized with TS (Fig. 3), as 50% inhibitory concentration (IC_{50}) isobolograms showed that all combinations were below the line of additivity. Combination indices (CIs) were less than 1 (Fig. 3E). Based on the checkerboards, isobolograms, and CI values, CO and CLI demonstrated the most potent synergy with TS while GN had the weakest. Attempts to combine GN with DSX or CO resulted in antagonism, likely due to the chelators binding Ga^{3+} (see Fig. S2).

Each compound potentiates TS activity. We previously showed that iron chelation potentiates the effects of TS, as DSX alone has no anti-*Pseudomonas* activity (21). CLI, TRO, DOXY, and CO inhibit *P. aeruginosa* growth, suggesting that the innate activity of the compounds could be partly responsible for synergy with TS. Thus, we considered four potential mechanisms of synergy. (i) TS potentiates the activity of each compound
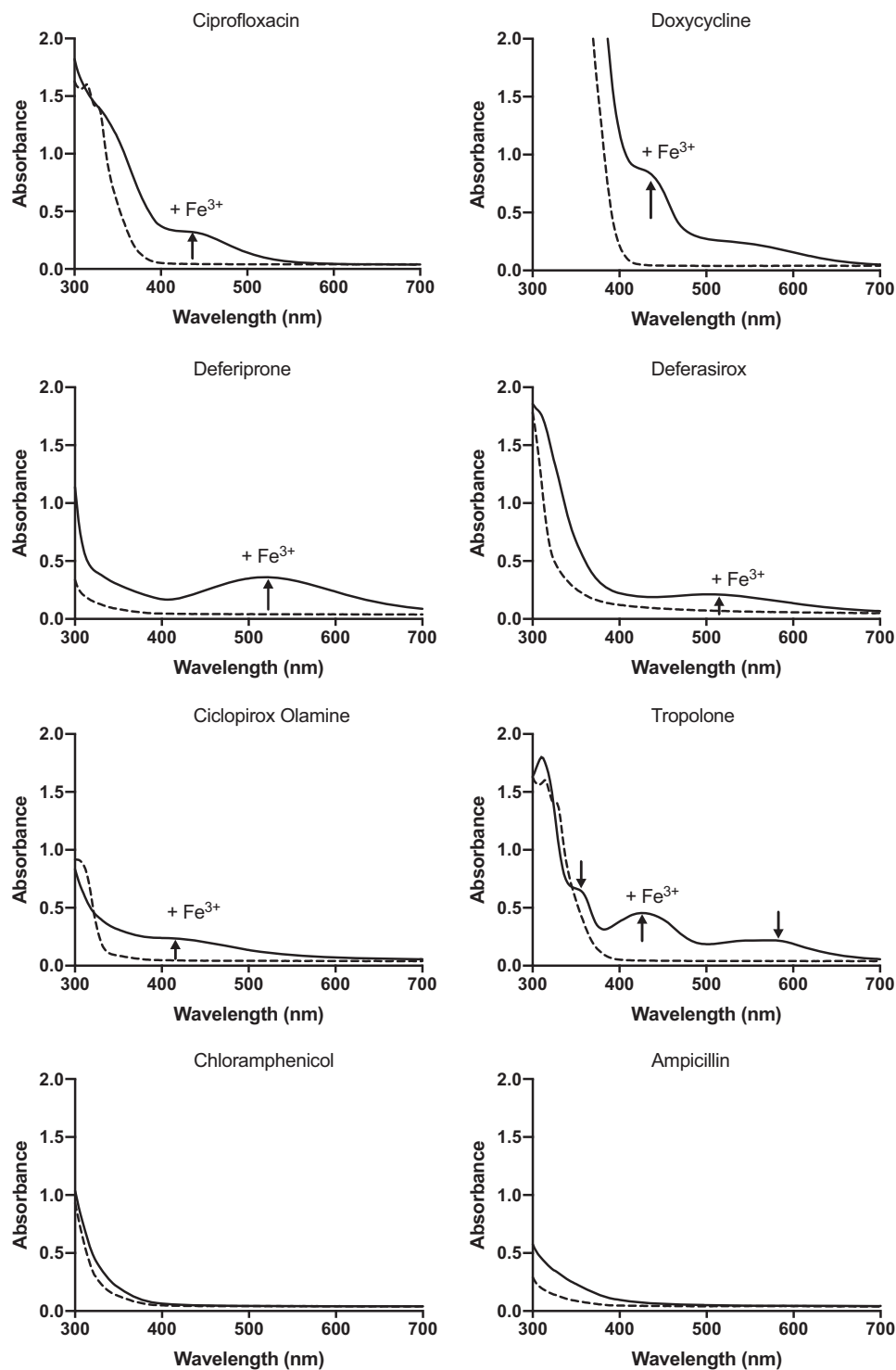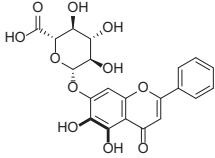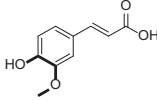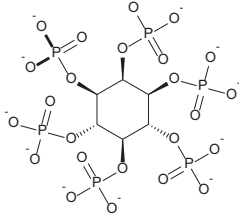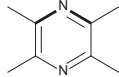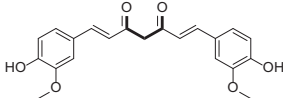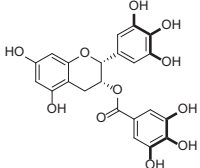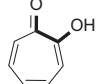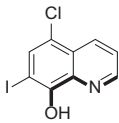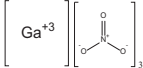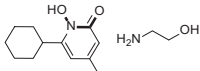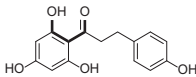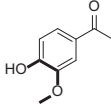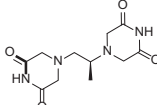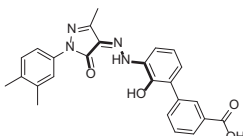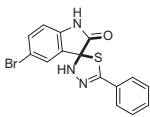
FIG 2 UV-visible absorption spectra of compounds with and without Fe(III). Equimolar concentrations of compound and $FeCl_3$ were added in deionized H_2O to a final concentration of 300 μM, and spectra of wavelengths from 300 nm to 700 nm were read after 1 h of incubation at room temperature. The black dashed lines are the spectra of the compounds in the absence of iron. The black solid lines are the spectra after the addition of iron. New peaks appearing after the addition of Fe^{3+} are indicated with arrows. Chloramphenicol and ampicillin were used as negative controls. Each assay was performed at least 3 times, and averaged values are shown.

TABLE 1 The structures of literature-derived compounds used in this study with potential iron chelation sites bolded

Compound	Structure	Description	Reference(s)
Baicalin		Flavonoid isolated from the Chinese herb *Scutellaria baicalensis* with antioxidant, anti-inflammatory, and anticancer activity	37–39
Ferulic acid		Natural product found in plant cell walls with antioxidant activity	40–42
Sodium phytate		Naturally occurring compound found in wheat and rice with anticancer and antioxidant activity	43–45
2,3,5,6-Tetramethylpyrazine		Alkaloid derived from the Chinese herb *Ligusticum wallichii* that is used to treat vascular diseases	40
Curcumin		Natural product of turmeric with anticancer activity	46, 47
Epigallocatechin gallate		Polyphenol isolated from green tea extract	41, 48–50
Tropolone		Synthetic compound with broad-spectrum antimicrobial activity	51, 52
Clioquinol		Used to treat fungal and bacterial infections; also used in the treatment of Alzheimer's disease	36, 39, 47, 53
Gallium nitrate		Iron analogue with antimicrobial activity	54–56
Ciclopirox olamine		Antifungal agent	57, 58

(Continued on next page)

TABLE 1 (Continued)

Compound	Structure	Description	Reference(s)
Phloretin		Flavonoid found in apples and pears	59, 60
Apocynin		NADPH-oxidase inhibitor	41, 61
Dexrazoxane		Cardioprotective agent	62, 63
Eltrombopag		Thrombopoietin receptor agonist used to treat thrombocytopenia	64–66
Lipofermata		Fatty acid transport inhibitor	67

through an unknown mechanism. (ii) The compound potentiates TS activity by chelating calcium and magnesium and increasing outer membrane permeability or (iii) by chelating iron and increasing TS uptake. In all these cases, the synergy is unidirectional. (iv) TS and the compound potentiate one another through an unknown mechanism.

Our data suggest that the synergy between TS and each compound is due to their iron chelation capacity rather than membrane permeabilization. First, to determine if DOXY can increase outer membrane permeability, vancomycin (VAN) and DOXY combinations were tested against PA14 alone or in the presence of Ca^{2+}, Mg^{2+}, or Fe^{3+} (see Fig. S3). VAN was selected because it is similar to TS in size but, unlike TS, its activity is unrelated to iron availability. VAN has a high MIC against *P. aeruginosa* due to limited uptake across the outer membrane. If a compound increases membrane permeability, we expect synergy with VAN. In our checkerboard assays, no synergy was identified for VAN plus DOXY, VAN plus CLI, VAN plus CO, or VAN plus TRO. Furthermore, the addition of 100 μM Mg^{2+} or Ca^{2+} had no effect on the checkerboard profiles compared to that of the control. In contrast, the addition of 100 μM Fe^{3+} abrogated the inhibitory activity of CLI, TRO, and CO, confirming that iron chelation is a critical part of the mechanism by which those compounds impede growth. Lack of synergy between VAN plus DOXY also suggested lack of membrane permeabilization. The addition of 100 μM Mg^{2+} had no effect on the checkerboard, whereas the addition of Fe^{3+} and Ca^{2+} had a negligible effect. This is reflective of the relatively weak ability of DOXY to compete for iron in the CAS assay (Fig. S1) and of its weak synergy with TS compared to that of other compounds.

To test the hypothesis that the compounds potentiate TS activity, rather than the other way around, three-dimensional (3D) checkerboard assays were performed using PA14. The surface area of each checkerboard was expressed as a percentage of control and graphed against the concentration of the third compound (see Fig. S4). Individual MIC assays for each compound were performed, and the results were graphed as percentages of control on the same y axis on a $\log_{10}$ scale. Significant differences
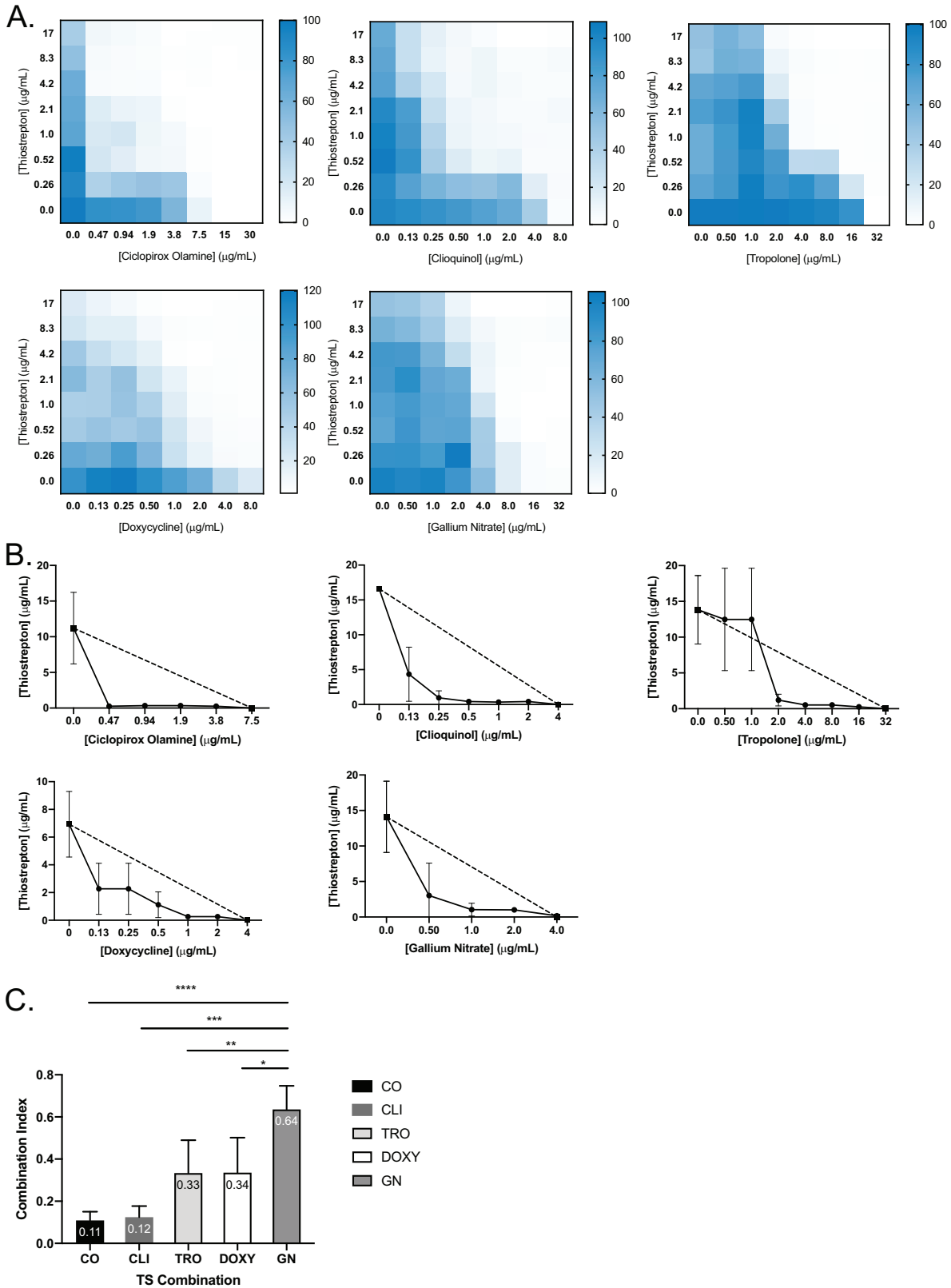
FIG 3 Iron chelators are synergistic with TS against *P. aeruginosa* PA14. Checkerboards (A) and IC$_{50}$ isobolograms (B) are shown for each compound that synergized with TS. Dashed lines indicate the lines of additivity, and solid lines indicate the IC$_{50}$s of TS at each compound concentration. Checkerboards and IC$_{50}$ isobolograms are arranged in the following order: CO, CLI, TRO, DOXY, and GN from left to right, top to bottom. (C) Combination indices (CI) of each TS combination. CI values are indicated at the top of the bars. All experiments were conducted 3 times. Average values are reported. ****, $P < 0.0001$; ***, $P < 0.001$; **, $P < 0.01$; *, $P < 0.05$.

between the two data sets would indicate that the TS plus DSX combination potentiates the activity of the test compound. To account for potential antagonism between test compounds and DSX, two-dimensional (2D) checkerboard assays were conducted (see Fig. S5). DSX plus TRO and DSX plus CO were indifferent. CLI antagonized with DSX at the MIC; however, we could not test concentrations of CLI greater than 8 μg/ml due to its poor solubility. DSX was additive with DOXY. We saw no significant differences between the activity of the chelators alone and in combination with TS and DSX, except for with CLI (Fig. 4A to D). CLI antagonized DSX at the highest concentration; however, growth was still below 20% of control (Fig. 4C), which we previously established as equivalent to the MIC in the growth medium used for this work (21). When the data were plotted against TS concentration (Fig. 4E), significant differences for the combinations were apparent at 2 and 4 μg/ml TS compared to TS alone, indicating that the compounds and DSX potentiate TS activity. These data suggest that the synergy between the chelators and TS is unidirectional.

TS combinations are bactericidal and effective against clinical isolates. TS, CO, CLI, DOXY, and TRO alone were bacteriostatic; however, when combined with TS, the combinations were bactericidal (see Fig. S6). This improved activity prompted us to test the combinations against clinical isolates. Double (TS plus compound) and triple (TS plus DSX plus compound) combinations were tested against same panels of *P. aeruginosa* and *A. baumannii* clinical isolates we previously assayed for susceptibility to TS plus DSX (Fig. 5) (21). GN was omitted due to its weak synergy with TS against PA14 and antagonism with iron chelators (Fig. S2). TS and DSX were used at 8.3 μg/ml (5 μM) and 32 μg/ml as before, while the other compounds were added at one-eighth the MIC of PA14, corresponding to DOXY, CO, TRO, and CLI concentrations of 1 μg/ml, 2 μg/ml, 4 μg/ml, and 1 μg/ml, respectively.

Of the double combinations, TS plus DSX was the most potent against *P. aeruginosa* (Fig. 5A), consistent with our checkerboard assays. Interestingly, TS plus DOXY and TS plus CO had similar potencies despite differences in their CI values (Fig. 3). TS plus TRO was the least potent of the double combinations. TS plus CLI potency was similar to that of TS plus DSX, and this combination reduced the growth of our most resistant clinical isolate, C0379, while TS plus DSX did not. TS synergized with CLI to inhibit C0379 although a higher concentration (8 μg/ml) of CLI was required (Fig. 6). Of the triple combinations, TS plus DSX plus DOXY was the most potent, with only C0379 showing resistance. We previously reported that C0379 has a partial deletion of *fpvB*, encoding a pyoverdine receptor (21). However, triple combinations with higher concentrations of DOXY and CO were able to inhibit its growth (Fig. 6A and C). C0379 growth was also inhibited by TS plus CLI or TS plus DSX plus CLI, if CLI was used at 8 μg/ml. CLI alone did not reduce growth below MIC and there was no antagonism between DSX and CLI with C0379 compared to that with PA14 (Fig. 6B). C0379 was also less susceptible to TRO than PA14 (Fig. 6D).

For *A. baumannii* isolates, all double combinations were equally effective. TS plus CLI was highly potent against *A. baumannii* compared to *P. aeruginosa* when CLI was used at 1 μg/ml (Fig. 5B and S7). Strain C0286 was resistant to TS but susceptible to TS plus CLI, suggesting inhibition was due to CLI. Conversely, TS plus TRO had little activity against *P. aeruginosa* clinical isolates but was effective against *A. baumannii*. The triple combinations inhibited the growth of both species.

DISCUSSION

A diverse repertoire of iron uptake mechanisms allows *P. aeruginosa* to proliferate under iron-limited conditions, similar to those encountered during infection of a host. Thus, repurposing iron chelators as antibiotic adjuvants may increase the expression of iron uptake pathways that can then be exploited to deliver antibacterial compounds. Both *P. aeruginosa* and *A. baumannii* express pyoverdine receptors FpvA and FpvB, which are highly upregulated under iron-limited conditions (6, 7). TS hijacks these pyoverdine receptors to enter the cell, as mutants lacking both receptors are resistant. The combination of TS plus DSX inhibited the growth of most clinical isolates (21). Here,
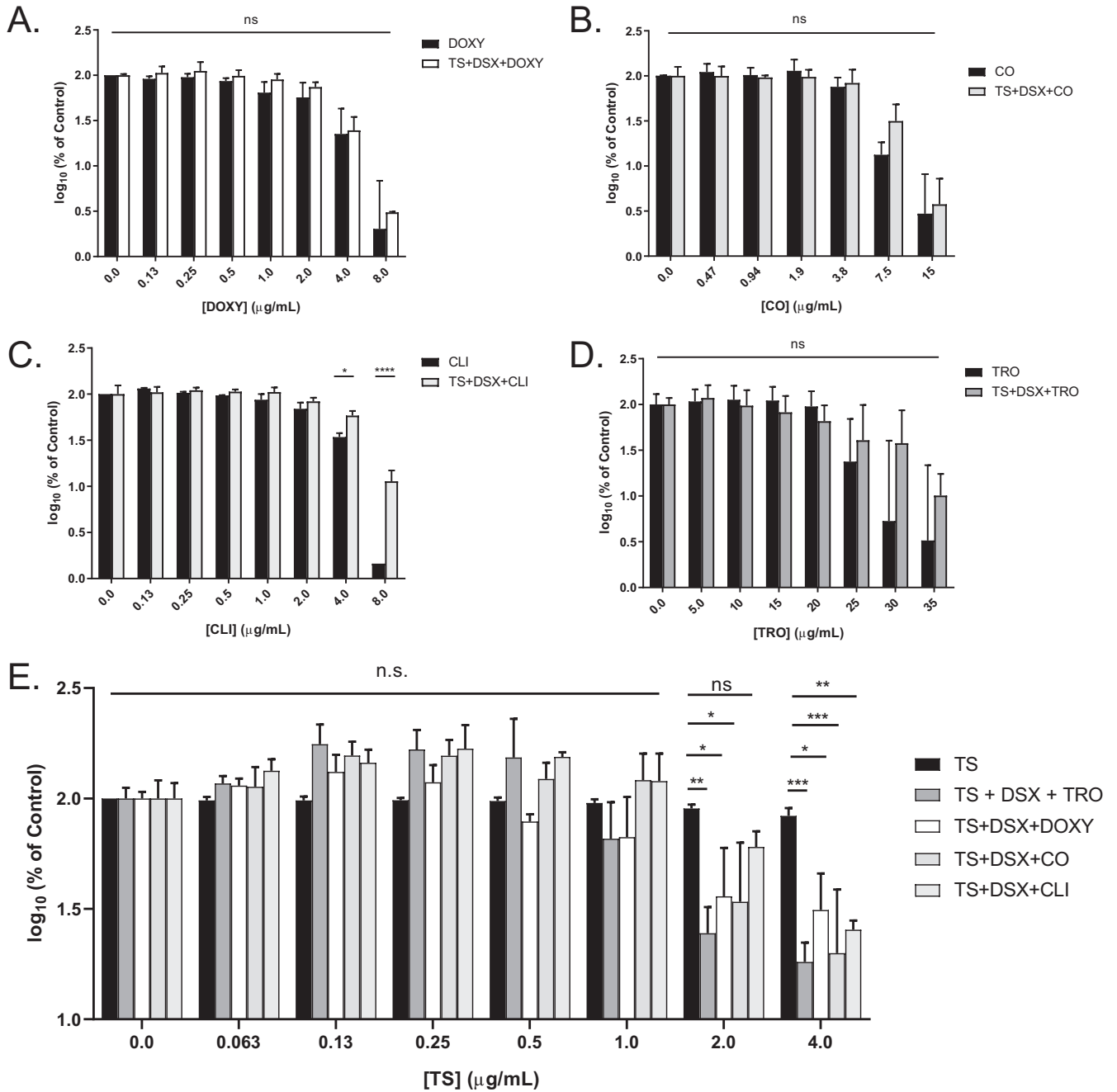
FIG 4 Unidirectional synergy between chelators and TS. Surface areas of 3D checkerboards were plotted against chelator concentration in terms of percentage of control on a $\log_{10}$ scale and compared to the activity of each chelator alone: DOXY (A), CO (B), and CLI (C). As shown in Fig. S4 in the supplemental material, CLI antagonized with DSX against PA14; thus, the triple combination allowed more growth than CLI alone at its highest concentration. However, the triple combination reduced growth below the previously established MIC, 20% of control (20). (D) TRO. (E) Surface areas were graphed with respect to increasing TS concentrations and compared to the activity of TS alone. n.s., not significantly different; *, $P < 0.05$; **, $P < 0.005$; ***, $P < 0.0005$. The averages from at least three biological replicates are shown.

we identified additional iron-chelating compounds that synergize with TS to inhibit the growth of the few clinical isolates that were resistant to TS plus DSX.

Antimicrobial-iron chelator combinations have been explored for treatment of both bacterial and fungal infections. A combination of DSX and tobramycin inhibited *P. aeruginosa* biofilm formation on cystic fibrosis (CF) airway cells (26), while chelation of iron by DOXY potentiated the activity of fluconazole against *Candida albicans* (27). For *P. aeruginosa*, iron restriction has the added benefit of increasing twitching motility and reducing biofilm formation, leaving cells more susceptible to antibiotic treatment (28).
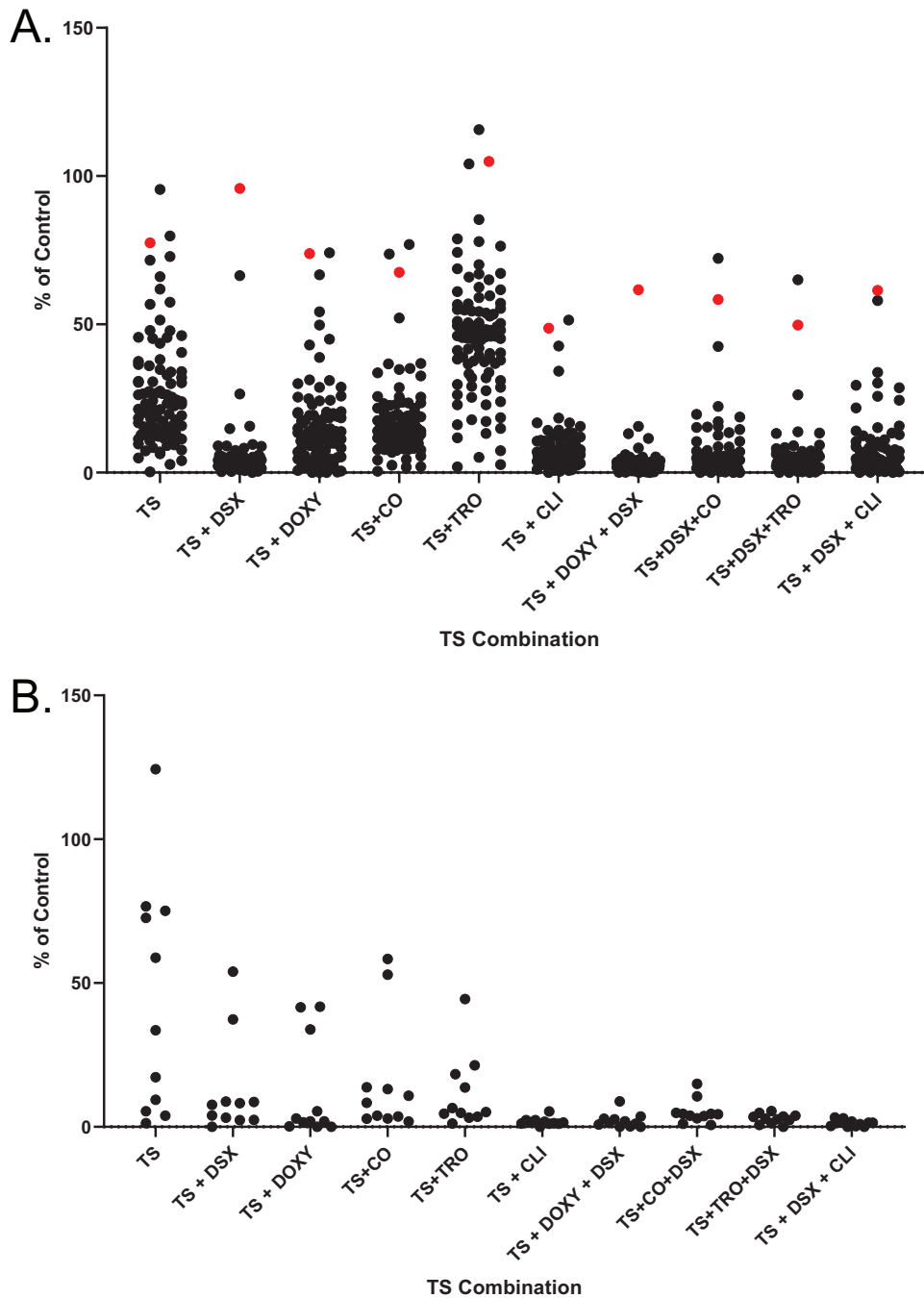
FIG 5 TS combinations inhibit the growth of clinical isolates. Single, double, and triple TS combinations were used to inhibit the growth of *P. aeruginosa* (A) and *A. baumannii* (B) clinical isolates. Highly resistant strain C0379 is highlighted in red. TS and DSX were used at 8.3 μg/ml and 32 μg/ml, respectively. The third compound was used at one-fourth MIC against PA14 (1 μg/ml DOXY, 2 μg/ml CO, 4 μg/ml TRO, and 1 μg/ml CLI). Assays were performed at least 3 times.

Here, we identified multiple compounds that synergize with TS against *P. aeruginosa* and *A. baumannii* clinical isolates due to their ability to chelate iron. Iron-binding capacity was demonstrated by monitoring visual color changes when complexed with Fe^{3+}, CAS agar decolorization, and via spectrophotometric assays. The CAS assay, which is used to detect siderophore production, not only indicates whether a compound can bind iron, but also if it has a stronger affinity for the metal than the CAS-HDTMA complex. This allowed us to compare the relative binding affinities of various com-

FIG 6 Growth of highly resistant strain C0379 is inhibited with increased concentrations of CO, CLI, and DOXY. The resistant clinical isolate was challenged with single, double, a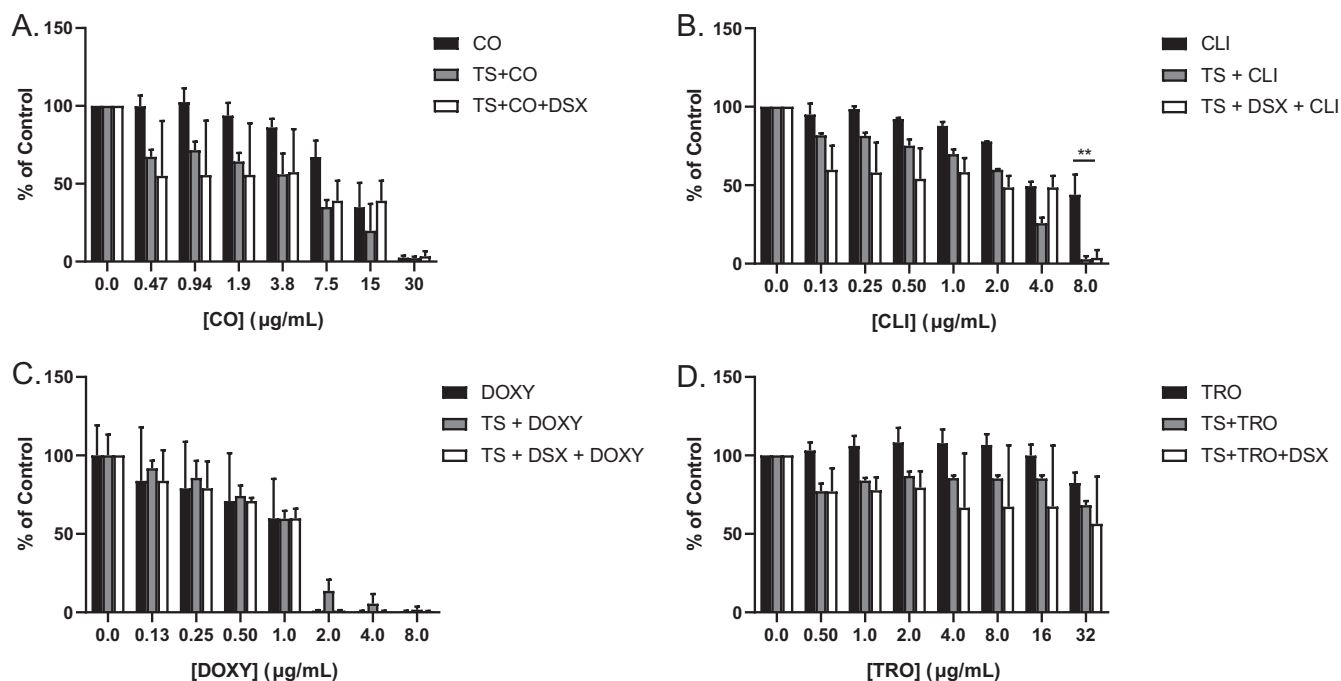nd triple combinations of CO (A), CLI (B), DOXY (C), and TRO (D). Increasing doses of each compound were combined with TS and DSX at 8.3 μg/ml and 32 μg/ml, respectively. MIC assays were conducted at least 3 times and averaged results are shown. **, $P < 0.001$.

pounds based on the extent of decolorization. This method is limited by compound solubility, as seen with CLI (see Fig. S1 in the supplemental material).

None of the natural phytochelators from plants that we tested, including baicalin, ferulic acid, sodium phytate, 2,3,5,6-tetramethylpyrazine, curcumin, epigallocatechin gallate, and phloretin (Table 1), synergized with TS. *P. aeruginosa* can act as a plant pathogen and may have evolved to outcompete or even take up phytochelators (29–32). The compounds that synergized with TS are all synthetic, and the extent of synergy correlated with their ability to strip iron from CAS-Fe^{3+}-HDTMA complexes (Fig. 3 and S1). Iron chelators compete with siderophores and reduce iron availability, resulting in increased pyoverdine receptor expression and susceptibility to TS (33). Weaker chelators such as DOXY and CIP showed little or no synergy with TS, whereas strong chelators such as CO and TRO exhibited greater synergy.

The GN data demonstrate that synergy with TS can occur via routes other than iron chelation. Ga^{3+} represses pyoverdine production and forms complexes with pyoverdine that prevent iron binding (25, 34). TS activity could be weakly potentiated because of reduced competition for pyoverdine receptors if siderophore production decreases upon GN treatment. These data show that disrupting iron acquisition may be another avenue for novel TS combinations. GN in triple combinations with TS plus chelator has limited utility because iron chelators bind Ga^{3+} (Fig. S2). However, one study showed that LK11, a compound that inhibits pyoverdine function directly, sensitized cells to CO to the same extent as a pyoverdine null mutant (35). Our previous work showed that a PA14 *pvdA* transposon mutant was more susceptible to TS than the wild type, which suggests that pyoverdine biosynthesis inhibitors could be useful TS adjuvants (21).

In summary, TS synergizes with iron-chelating compounds of diverse structures that were not primarily intended as antibacterial compounds. For example, CLI has antifungal and antiprotozoal properties and was investigated as a potential treatment for Alzheimer's disease; however, the compound was shown to be neurotoxic at higher concentrations (36). CO is also used as a topical antifungal agent. Given that *P. aeruginosa* is a burn wound pathogen and the precedence of these chelators as topical agents, the combinations we identified may be useful in treating superficial infections

caused by this pathogen. Although the mechanisms of action for some of these molecules are not fully understood, they may reveal new targets for antibiotic therapy. In addition, TS combinations demonstrated bactericidal activity while chelator compounds alone were bacteriostatic. The new combinations were effective against clinical isolates resistant to TS plus DSX. We note that the combinations were more potent against *A. baumannii* isolates than those of *P. aeruginosa* (Fig. 5). Further study with a larger sample size of *A. baumannii* isolates is needed to confirm these results. It is possible that there are differences in pyoverdine receptor density or affinity for TS between the two species that lead to increased uptake by *A. baumannii*. To keep the concentrations of the chelators in the combinations consistent, one-eighth the MIC against *P. aeruginosa* PA14 was used. It is possible that the MICs of the *A. baumannii* clinical isolates were intrinsically lower. Our data suggest that these compounds have dual roles, as antibacterial agents and TS adjuvants. Iron restriction mimics many *in vivo* conditions, as host proteins sequester free iron in an attempt to starve bacteria and exert antibacterial activity. Screening for antibiotic activity under similar conditions is an important strategy for the development of new treatments for the most dangerous pathogens.

MATERIALS AND METHODS

Bacterial strains, compounds, and culture conditions. *P. aeruginosa* PA14 was used for checkerboard assays as previously described (21). All clinical isolates were from the Wright Clinical Collection as described previously. Bacterial overnight cultures were grown in lysogeny broth (LB) and subcultured in 10:90 medium (10% LB, 90% phosphate-buffered saline [PBS]). All growth assays were performed using 10:90 with growth for 16 h at 37°C and 200 rpm. Compounds from Table 1 were from AK Scientific, Sigma, and Cayman Chemicals. TS and DSX were from Cayman Chemicals and AK Scientific, respectively. Compounds were stored at −20°C. Stock solutions were stored at −20°C until use except for the tetracyclines, which were made fresh due to precipitation at −20°C.

Absorption spectrum assays for iron chelation. Compounds were arrayed in Nunc 96-microwell plates. Vehicle controls contained Milli-Q H_2O with 1:75 dilutions of each compound at a final concentration of 300 μM. The experimental setup contained the same components as the vehicle control, with the addition of 300 μM $FeCl_3$. The final volume in each well was 150 μl. The plate was incubated at room temperature for 1 h, and absorption spectra from 300 nm to 700 nm were read in 2-nm increments (Multiskan Go; Thermo Fisher Scientific).

CAS assay. CAS agar plates were prepared as described previously (21). Compounds were standardized to 2 mg/ml, and 10 μl of each was spotted onto the plate. Plates were incubated at room temperature for 1 h and then photographed. Three replicates were conducted, and the image of a representative plate was presented.

Dose-response and checkerboard assays. Dose-response and checkerboard assays were conducted as described previously (21). Briefly, overnight cultures were grown in LB for 16 h at 37°C and 200 rpm and then subcultured (1:500 dilution) into 10:90 for 6 h. Subcultures were standardized to an optical density at 600 nm (OD_{600}) of 0.10 and diluted 1:500 in fresh 10:90 before use. For the dose-response assay, serial dilutions of compounds were added at 75 times the final concentration and diluted with 10:90 with cells to reach the desired final concentration. This was conducted in triplicates for technical replicates. Vehicle and sterile controls were included. The checkerboard assay was performed similarly to the dose-response assay but in an 8-by-8 format in a 96-well Nunc plate, with concentration of one drug increasing along the *y* axis and the other along the *x* axis. Sterility and vehicle controls were included with two columns allocated for each control. At least three biological replicates were repeated for the dose-response and checkerboard assays.

3D checkerboard assays. Three-dimensional checkerboard assays were performed in Nunc 96-microwell plates in an 8-by-8-by-8 matrix format for a total of 512 wells. The first two columns were used for the vehicle controls while the last two columns were allocated to sterility controls, both consisting of 2.7% (vol/vol) dimethyl sulfoxide (DMSO) plus 1.3% (vol/vol) H_2O for plates with TRO and DOXY and 4% (vol/vol) DMSO for plates with CLI and CO. Serial dilutions of TS were added along the *y* axis of each plate starting at 0 μg/ml, with the highest final concentration being 4 μg/ml. Serial dilutions of DSX were added along the *x* axis of each plate, from 0 μg/ml to the highest final concentration of 8 μg/ml. Serial dilutions of compounds were added with an increasing concentration in each plate up to a final concentration of 35 μg/ml (TRO), 8 μg/ml (DOXY), 30 μg/ml (CO), or 8 μg/ml (CLI) in the last plate. Each well contained 144 μl of 10:90 inoculated with PA14, except for the sterility control columns which contained 10:90 only. The final volume in each plate was 150 μl. The plates were sealed with parafilm and incubated at 37°C for 16 h with shaking at 200 rpm. The OD_{600} of the plates was read (Multiskan Go; Thermo Fisher Scientific). Each experiment was repeated at least three times. Checkerboards were analyzed in Excel. Representative plots at one-fourth MIC were made using MATLAB. Surface areas were averaged, expressed as percentage of control, and plotted against each compound concentration (Prism; GraphPad Software).

Clinical isolate testing. Isolates from the Wright Clinical Collection were grown and tested as described previously (21). Briefly, clinical isolates were inoculated from glycerol stocks stored at −80°C

into Nunc 96-well plates and grown overnight (for 16 h) at 37°C with shaking (200 rpm) in LB. Overnight cultures were subcultured (1:25) into fresh 10:90 medium and grown for 2 h under the same growth conditions. Subcultures were diluted 1:75 in fresh 10:90. Compounds were diluted 1:75 to obtain the final concentrations. DOXY and CLI were added at a final concentration of 1 μg/ml, CO was used at 2 μg/ml, TRO was used at 4 μg/ml, TS was used at 8.3 μg/ml, and DSX was used at 32 μg/ml. Vehicle and sterility controls were included. Plates were incubated overnight under the same conditions. The OD_{600}s were read (Multiskan Go; Thermo Fisher Scientific) and analyzed using Excel, and the data were plotted using Prism (GraphPad Software).

SUPPLEMENTAL MATERIAL

Supplemental material is available online only.

SUPPLEMENTAL FILE 1, PDF file, 3.6 MB.

ACKNOWLEDGMENTS

REFERENCES

1. Banin E, Vasil ML, Greenberg EP. 2005. From the Cover: Iron and *Pseudomonas aeruginosa* biofilm formation. Proc Natl Acad Sci U S A 102:11076–11081. https://doi.org/10.1073/pnas.0504266102.
2. Schaible UE, Kaufmann S. 2004. Iron and microbial infection. Nat Rev Microbiol 2:946–953. https://doi.org/10.1038/nrmicro1046.
3. Voulhoux R, Filloux A, Schalk IJ. 2006. Pyoverdine-mediated iron uptake in *Pseudomonas aeruginosa*: the Tat system is required for PvdN but not for FpvA transport. J Bacteriol 188:3317–3323. https://doi.org/10.1128/JB.188.9.3317-3323.2006.
4. Heinrichs DE, Young L, Poole K. 1991. Pyochelin-mediated iron transport in *Pseudomonas aeruginosa*: involvement of a high-molecular-mass outer membrane protein. Infect Immun 59:3680–3684.
5. Cornelis P, Matthijs S, Van Oeffelen L. 2009. Iron uptake regulation in *Pseudomonas aeruginosa*. Biometals 22:15–22. https://doi.org/10.1007/s10534-008-9193-0.
6. Gonzalez MR, Ducret V, Leoni S, Fleuchot B, Jafari P, Raffoul W, Applegate LA, Que Y-A, Perron K. 2018. Transcriptome analysis of *Pseudomonas aeruginosa* cultured in human burn wound exudates. Front Cell Infect Microbiol 8:39. https://doi.org/10.3389/fcimb.2018.00039.
7. Damron FH, Oglesby-Sherrouse AG, Wilks A, Barbier M. 2016. Dual-seq transcriptomics reveals the battle for iron during *Pseudomonas aeruginosa* acute murine pneumonia. Sci Rep 6:39172. https://doi.org/10.1038/srep39172.
8. Ratledge C, Dover LG. 2000. Iron metabolism in pathogenic bacteria. Annu Rev Microbiol 54:881–941. https://doi.org/10.1146/annurev.micro.54.1.881.
9. Meyer JM, Neely A, Stintzi A, Georges C, Holder IA. 1996. Pyoverdin is essential for virulence of *Pseudomonas aeruginosa*. Infect Immun 64:518–523.
10. Eckenroth BE, Steere AN, Chasteen ND, Everse SJ, Mason AB. 2011. How the binding of human transferrin primes the transferrin receptor potentiating iron release at endosomal pH. Proc Natl Acad Sci U S A 108:13089–13094. https://doi.org/10.1073/pnas.1105786108.
11. Kang D, Kirienko NV. 2017. High-throughput genetic screen reveals that early attachment and biofilm formation are necessary for full pyoverdine production by *Pseudomonas aeruginosa*. Front Microbiol 8:1707. https://doi.org/10.3389/fmicb.2017.01707.
12. Minandri F, Imperi F, Frangipani E, Bonchi C, Visaggio D, Facchini M, Pasquali P, Bragonzi A, Visca P. 2016. Role of iron uptake systems in *Pseudomonas aeruginosa* virulence and airway infection. Infect Immun 84:2324–2335. https://doi.org/10.1128/IAI.00098-16.
13. Denayer S, Matthijs S, Cornelis P. 2007. Pyocin S2 (Sa) kills *Pseudomonas aeruginosa* strains via the FpvA type I ferripyoverdine receptor. J Bacteriol 189:7663–7668. https://doi.org/10.1128/JB.00992-07.
14. Elfarash A, Wei Q, Cornelis P. 2012. The soluble pyocins S2 and S4 from *Pseudomonas aeruginosa* bind to the same FpvAI receptor. Microbiologyopen 1:268–275. https://doi.org/10.1002/mbo3.27.
15. Mislin GLA, Schalk IJ. 2016. Fluorescent aliphatic hyperbranched polyether: chromophore-free and without any N and P Atoms. Phys Chem Chem Phys 18:4295–4299. https://doi.org/10.1039/c5cp07134h.
16. Wittmann S, Schnabelrauch M, Scherlitz-Hofmann I, Möllmann U, Ankel-Fuchs D, Heinisch L. 2002. New synthetic siderophores and their beta-lactam conjugates based on diamino acids and dipeptides. Bioorg Med Chem 10:1659–1670. https://doi.org/10.1016/s0968-0896(02)00044-5.
17. Kline T, Fromhold M, McKennon TE, Cai S, Treiberg J, Ihle N, Sherman D, Schwan W, Hickey MJ, Warrener P, Witte PR, Brody LL, Goltry L, Barker LM, Anderson SU, Tanaka SK, Shawar RM, Nguyen LY, Langhorne M, Bigelow A, Embuscado L, Naeemi E. 2000. Antimicrobial effects of novel siderophores linked to beta-lactam antibiotics. Bioorg Med Chem 8:73–93. https://doi.org/10.1016/s0968-0896(99)00261-8.
18. Brochu A, Brochu N, Nicas TI, Parr TR, Minnick AA, Dolence EK, McKee JA, Miller MJ, Lavoie MC, Malouin F. 1992. Modes of action and inhibitory activities of new siderophore-beta-lactam conjugates that use specific iron uptake pathways for entry into bacteria. Antimicrob Agents Chemother 36:2166–2175. https://doi.org/10.1128/aac.36.10.2166.
19. Ito A, Sato T, Ota M, Takemura M, Nishikawa T, Toba S, Kohira N, Miyagawa S, Ishibashi N, Matsumoto S, Nakamura R, Tsuji M, Yamano Y. 2018. *In vitro* antibacterial properties of cefiderocol, a novel siderophore cephalosporin, against Gram-negative bacteria. Antimicrob Agents Chemother 62:e01454-17. https://doi.org/10.1128/AAC.01454-17.
20. Dobias J, Dénervaud-Tendon V, Poirel L, Nordmann P. 2017. Activity of the novel siderophore cephalosporin cefiderocol against multidrug-resistant Gram-negative pathogens. Eur J Clin Microbiol Infect Dis 36:2319–2327. https://doi.org/10.1007/s10096-017-3063-z.
21. Ranieri MRM, Chan DCK, Yaeger LN, Rudolph M, Karabelas-Pittman S, Abdo H, Chee J, Harvey H, Nguyen U, Burrows LL. 2019. Thiostrepton hijacks pyoverdine receptors to inhibit growth of *Pseudomonas aeruginosa*. Antimicrob Agents Chemother 60:e00472-19. https://doi.org/10.1128/AAC.00472-19.
22. Petit L, Adamo C, Russo N. 2005. Absorption spectra of first-row transition metal complexes of bacteriochlorins: a theoretical analysis. J Phys Chem B 109:12214–12221. https://doi.org/10.1021/jp050667d.
23. Sever MJ, Wilker JJ. 2004. Visible absorption spectra of metal–catecholate and metal–tironate complexes. Dalton Trans 4:1061–1072. https://doi.org/10.1039/B315811J.
24. Sutton D. 1969. Electronic spectra of transition metal complexes. J Electrochem Soc 116:310C. https://doi.org/10.1149/1.2412267.
25. Kaneko Y, Thoendel M, Olakanmi O, Britigan BE, Singh PK. 2007. The transition metal gallium disrupts *Pseudomonas aeruginosa* iron metabolism and has antimicrobial and antibiofilm activity. J Clin Invest 117:877–888. https://doi.org/10.1172/JCI30783.

26. Moreau-Marquis S, O'Toole GA, Stanton BA. 2009. Tobramycin and FDA-approved iron chelators eliminate *Pseudomonas aeruginosa* biofilms on cystic fibrosis cells. Am J Respir Cell Mol Biol 41:305–313. https://doi.org/10.1165/rcmb.2008-0299OC.

27. Fiori A, Van Dijck P. 2012. Potent synergistic effect of doxycycline with fluconazole against *Candida albicans* is mediated by interference with iron homeostasis. Antimicrob Agents Chemother 56:3785–3796. https://doi.org/10.1128/AAC.06017-11.

28. Singh PK, Parsek MR, Greenberg EP, Welsh MJ. 2002. A component of innate immunity prevents bacterial biofilm development. Nature 417:552–555. https://doi.org/10.1038/417552a.

29. Starkey M, Rahme LG. 2009. Modeling *Pseudomonas aeruginosa* pathogenesis in plant hosts. Nat Protoc 4:117–124. https://doi.org/10.1038/nprot.2008.224.

30. Rahme LG, Tan MW, Le L, Wong SM, Tompkins RG, Calderwood SB, Ausubel FM. 1997. Use of model plant hosts to identify *Pseudomonas aeruginosa* virulence factors. Proc Natl Acad Sci U S A 94:13245–13250. https://doi.org/10.1073/pnas.94.24.13245.

31. Green SK, Schroth MN, Cho JJ, Kominos SK, Vitanza-Jack VB. 1974. Agricultural plants and soil as a reservoir for *Pseudomonas aeruginosa*. Appl Microbiol 28:987–991. https://doi.org/10.1128/AEM.28.6.987-991.1974.

32. Gi M, Lee K-M, Kim SC, Yoon J-H, Yoon SS, Choi JY. 2015. A novel siderophore system is essential for the growth of *Pseudomonas aeruginosa* in airway mucus. Sci Rep 5:14644. https://doi.org/10.1038/srep14644.

33. Smith DJ, Lamont IL, Anderson GJ, Reid DW. 2013. Targeting iron uptake to control *Pseudomonas aeruginosa* infections in cystic fibrosis. Eur Respir J 42:1723–1736. https://doi.org/10.1183/09031936.00124012.

34. Ross-Gillespie A, Weigert M, Brown SP, Kümmerli R. 2014. Gallium-mediated siderophore quenching as an evolutionarily robust antibacterial treatment. Evol Med Public Health 2014:18–29. https://doi.org/10.1093/emph/eou003.

35. Kirienko DR, Kang D, Kirienko NV. 2018. Novel pyoverdine inhibitors mitigate *Pseudomonas aeruginosa* pathogenesis. Front Microbiol 9:3317. https://doi.org/10.3389/fmicb.2018.03317.

36. Benvenisti-Zarom L, Chen J, Regan RF. 2005. The oxidative neurotoxicity of clioquinol. Neuropharmacology 49:687–694. https://doi.org/10.1016/j.neuropharm.2005.04.023.

37. Perez CA, Wei Y, Guo M. 2009. Iron-binding and anti-Fenton properties of baicalein and baicalin. J Inorg Biochem 103:326–332. https://doi.org/10.1016/j.jinorgbio.2008.11.003.

38. Zhang Y, Li H, Zhao Y, Gao Z. 2006. Dietary supplementation of baicalin and quercetin attenuates iron overload induced mouse liver injury. Eur J Pharmacol 535:263–269. https://doi.org/10.1016/j.ejphar.2006.01.067.

39. Zhao Y, Li H, Gao Z, Xu H. 2005. Effects of dietary baicalin supplementation on iron overload-induced mouse liver oxidative injury. Eur J Pharmacol 509:195–200. https://doi.org/10.1016/j.ejphar.2004.11.060.

40. Hatcher HC, Singh RN, Torti FM, Torti SV. 2009. Synthetic and natural iron chelators: therapeutic potential and clinical use. Future Med Chem 1:1643–1670. https://doi.org/10.4155/fmc.09.121.

41. Hynes MJ, Ó Coinceanainn M. 2002. Investigation of the release of iron from ferritin by naturally occurring antioxidants. J Inorg Biochem 90:18–21. https://doi.org/10.1016/S0162-0134(02)00383-5.

42. Boyer RF, Clark HM, LaRoche AP. 1988. Reduction and release of ferritin iron by plant phenolics. J Inorg Biochem 32:171–181. https://doi.org/10.1016/0162-0134(88)80025-4.

43. Xu Q, Kanthasamy AG, Reddy MB. 2008. Neuroprotective effect of the natural iron chelator, phytic acid in a cell culture model of Parkinson's disease. Toxicology 245:101–108. https://doi.org/10.1016/j.tox.2007.12.017.

44. Minihane AM, Rimbach G. 2002. Iron absorption and the iron binding and anti-oxidant properties of phytic acid. Int J Food Sci Tech 37:741–748. https://doi.org/10.1046/j.1365-2621.2002.00619.x.

45. Kamp DW, Israbian VA, Panos RJ, Yeldandi AV, Graceffa P, Weitzman SA. 1995. Phytic acid, an iron chelator, attenuates pulmonary inflammation and fibrosis in rats after intratracheal instillation of asbestos. Toxicol Pathol 23:689–695. https://doi.org/10.1177/019262339502300606.

46. Jiao Y, Wilkinson J, Di X, Wang W, Hatcher H, Kock ND, D'Agostino R, Knovich MA, Torti FM, Torti SV. 2009. Curcumin, a cancer chemopreventive and chemotherapeutic agent, is a biologically active iron chelator. Blood 113:462–469. https://doi.org/10.1182/blood-2008-05-155952.

47. Baum L, Ng A. 2004. Curcumin interaction with copper and iron suggests one possible mechanism of action in Alzheimer's disease animal models. J Alzheimers Dis 6:367–377. https://doi.org/10.3233/jad-2004-6403.

48. Weinreb O, Amit T, Mandel S, Youdim M. 2009. Neuroprotective molecular mechanisms of (-)-epigallocatechin-3-gallate: a reflective outcome of its antioxidant, iron chelating and neuritogenic properties. Genes Nutr 4:283–296. https://doi.org/10.1007/s12263-009-0143-4.

49. Mandel SA, Amit T, Kalfon L, Reznichenko L, Weinreb O, Youdim M. 2008. Cell signaling pathways and iron chelation in the neurorestorative activity of green tea polyphenols: special reference to epigallocatechin gallate (EGCG). J Alzheimers Dis 15:211–222. https://doi.org/10.3233/jad-2008-15207.

50. Higuchi A, Yonemitsu K, Koreeda A, Tsunenari S. 2003. Inhibitory activity of epigallocatechin gallate (EGCg) in paraquat-induced microsomal lipid peroxidation - a mechanism of protective effects of EGCg against paraquat toxicity. Toxicology 183:143–149. https://doi.org/10.1016/s0300-483x(02)00512-7.

51. Azegami K, Nishiyama K, Kato H. 1988. Effect of iron limitation on "*Pseudomonas plantarii*" growth and tropolone and protein production. Appl Environ Microbiol 54:844–847. https://doi.org/10.1128/AEM.54.3.844-847.1988.

52. Ganeshaguru K, Hoffbrand AV, Grady RW, Cerami A. 1980. Effect of various iron chelating agents on DNA synthesis in human cells. Biochem Pharmacol 29:1275–1279. https://doi.org/10.1016/0006-2952(80)90285-3.

53. Shekhar-Guturja T, Gunaherath GMKB, Wijeratne EMK, Lambert J-P, Averette AF, Lee SC, Kim T, Bahn Y-S, Tripodi F, Ammar R, Döhl K, Niewola-Staszkowska K, Schmitt L, Loewith RJ, Roth FP, Sanglard D, Andes D, Nislow C, Coccetti P, Gingras A-C, Heitman J, Gunatilaka AAL, Cowen LE. 2016. Dual action antifungal small molecule modulates multidrug efflux and TOR signaling. Nat Chem Biol 12:867–875. https://doi.org/10.1038/nchembio.2165.

54. Chitambar CR. 2017. The therapeutic potential of iron-targeting gallium compounds in human disease: from basic research to clinical application. Pharmacol Res 115:56–64. https://doi.org/10.1016/j.phrs.2016.11.009.

55. De Léséleuc L, Harris G, KuoLee R, Chen W. 2012. *In vitro* and *in vivo* biological activities of iron chelators and gallium nitrate against *Acinetobacter baumannii*. Antimicrob Agents Chemother 56:5397–5400. https://doi.org/10.1128/AAC.00778-12.

56. Olakanmi O, Britigan BE, Schlesinger LS. 2000. Gallium disrupts iron metabolism of mycobacteria residing within human macrophages. Infect Immun 68:5619–5627. https://doi.org/10.1128/iai.68.10.5619-5627.2000.

57. Wu J, Liu H, Zhang G, Gu L, Zhang Y, Gao J, Wei Y, Ma Z. 2016. Antileukemia effect of ciclopirox olamine is mediated by downregulation of intracellular ferritin and inhibition β-catenin-c-Myc signaling pathway in glucocorticoid resistant T-ALL cell lines. PLoS One 11:e0161509. https://doi.org/10.1371/journal.pone.0161509.

58. Eberhard Y, McDermott SP, Wang X, Gronda M, Venugopal A, Wood TE, Hurren R, Datti A, Batey RA, Wrana J, Antholine WE, Dick JE, Dick J, Schimmer AD. 2009. Chelation of intracellular iron with the antifungal agent ciclopirox olamine induces cell death in leukemia and myeloma cells. Blood 114:3064–3073. https://doi.org/10.1182/blood-2009-03-209965.

59. Vlachodimitropoulou E, Sharp PA, Naftalin RJ. 2011. Quercetin-iron chelates are transported via glucose transporters. Free Radic Biol Med 50:934–944. https://doi.org/10.1016/j.freeradbiomed.2011.01.005.

60. van Acker SA, van Balen GP, van den Berg DJ, Bast A, van der Vijgh WJ. 1998. Influence of iron chelation on the antioxidant activity of flavonoids. Biochem Pharmacol 56:935–943. https://doi.org/10.1016/S0006-2952(98)00102-6.

61. Sharma S, Pal R, Hameed S, Fatima Z. 2016. Antimycobacterial mechanism of vanillin involves disruption of cell-surface integrity, virulence attributes, and iron homeostasis. Int J Mycobacteriol 5:460–468. https://doi.org/10.1016/j.ijmyco.2016.06.010.

62. Hasinoff BB, Patel D, Wu X. 2003. The oral iron chelator ICL670A (deferasirox) does not protect myocytes against doxorubicin. Free Radic Biol Med 35:1469–1479. https://doi.org/10.1016/j.freeradbiomed.2003.08.005.

63. Schroeder PE, Hasinoff BB. 2002. The doxorubicin-cardioprotective drug dexrazoxane undergoes metabolism in the rat to its metal ion-chelating form ADR-925. Cancer Chemother Pharmacol 50:509–513. https://doi.org/10.1007/s00280-002-0538-z.

64. Vlachodimitropoulou E, Chen Y-L, Garbowski M, Koonyosying P, Psaila B, Sola-Visner M, Cooper N, Hider R, Porter J. 2017. Eltrombopag: a powerful chelator of cellular or extracellular iron(III) alone or combined with a second chelator. Blood 130:1923–1933. https://doi.org/10.1182/blood-2016-10-740241.

65. Bastian TW, Duck KA, Michalopoulos GC, Chen MJ, Liu ZJ, Connor JR, Lanier LM, Sola-Visner MC, Georgieff MK. 2017. Eltrombopag, a thrombopoietin mimetic, crosses the blood–brain barrier and impairs iron-dependent hippocampal neuron dendrite development. J Thromb Haemost 15:565–574. https://doi.org/10.1111/jth.13602.

66. Roth M, Will B, Simkin G, Narayanagari S, Barreyro L, Bartholdy B, Tamari R, Mitsiades CS, Verma A, Steidl U. 2012. Eltrombopag inhibits the proliferation of leukemia cells via reduction of intracellular iron and induction of differentiation. Blood 120:386–394. https://doi.org/10.1182/blood-2011-12-399667.

67. Falconer SB, Wang W, Gehrke SS, Cuneo JD, Britten JF, Wright GD, Brown ED. 2014. Metal-induced isomerization yields an intracellular chelator that disrupts bacterial iron homeostasis. Chem Biol 21:136–145. https://doi.org/10.1016/j.chembiol.2013.11.007.

68. Ito A, Nishikawa T, Matsumoto S, Yoshizawa H, Sato T, Nakamura R, Tsuji M, Yamano Y. 2016. Siderophore cephalosporin cefiderocol utilizes ferric iron transporter systems for antibacterial activity against Pseudomonas aeruginosa. Antimicrob Agents Chemother 60:7396–7401. https://doi.org/10.1128/AAC.01405-16.